Photochemical & Photobiological Sciences

Accepted Manuscript

This is an *Accepted Manuscript*, which has been through the Royal Society of Chemistry peer review process and has been accepted for publication.

Accepted Manuscripts are published online shortly after acceptance, before technical editing, formatting and proof reading. Using this free service, authors can make their results available to the community, in citable form, before we publish the edited article. We will replace this *Accepted Manuscript* with the edited and formatted *Advance Article* as soon as it is available.

You can find more information about *Accepted Manuscripts* in the Information for Authors.

Please note that technical editing may introduce minor changes to the text and/or graphics, which may alter content. The journal's standard Terms & Conditions and the Ethical guidelines still apply. In no event shall the Royal Society of Chemistry be held responsible for any errors or omissions in this *Accepted Manuscript* or any consequences arising from the use of any information it contains.

ROYAL SOCIETY OF CHEMISTRY

www.rsc.org/pps

Journal Name

RSCPublishing

ARTICLE

Photophysical properties of electron-deficient free-base corrole bearing meso-fluorophenyl substituents.

Cite this: DOI: 10.1039/xoxxoooooox

Lei Zhang[a] , Zi-Yu Liu [a], Xuan Zhan,[b] Li-Li Wang[a], Hui Wang,[a*] and Hai-Yang Liu[b*]

Received ooth January 2012,
Accepted ooth January 2012

DOI: 10.1039/xoxxoooooox

www.rsc.org/

ABSTRACT: The ultrafast photophysical behaviors of a series of meso-flurophenyl substituted electron-deficient free base corroles F_0C, F_5C, $F_{10}C$ and $F_{15}C$ in toluene have been investigated using femtosecond time resolved absorption spectroscopy and steady spectroscopies. The $S_2 \rightarrow S_1^*$ transformation was found to be accelerated with the enhancement of electron-deficient virtue (from 550 fs for F_0C to 140 fs for $F_{15}C$), while $S_1^* \rightarrow S_1$ was prolonged from ~ 9 ps for F_0C to ~ 24 ps for $F_{15}C$, which was assigned to an intermolecular vibrational cooling process. The intersystem crossing process was directly observed. The intersystem crossing rate constant (k_{ISC}) from S_1 to T_1 was found to increase significantly with the flurophenyl substituents (from F_0C to $F_{10}C$), while it does not totally follow the trend of the increase of the atomic number of the peripherally fluorine atoms. The total sequence of ISC time constants from larger to smaller is: $F_0C < F_5C < F_{10}C > F_{15}C$. It indicates that the electron-withdrawing of flurophenyl substitutions, together with heavy atom effect, influence the photophysical properties of excited states of corroles.

Introduction:

Corrole is the close analogue of porphyrin, its symmetry decreases from D_{2h} of free-base porphyrin to C_s due to the lack of a meso methine unit. Also, corrole has more electron-rich π-system and a smaller core than porphyrin.[1] Photophysical properties of corrole have attracted much interests in recent years due to its potential uses in photodynamic therapy (PDT), photodynamic diagnosis (PDD), [2, 3] dye-sensitized solar cells[4], catalysis [5] and corrole-base electron and erengy transfer systems. [6-10]

Corrole designed for PDT should exhibit high singlet oxygen quantum yield, efficient intersystem crossing and long triplet state lifetime, while for use in PDD, it should present high fluorescence quantum yields. Previous research revealed the lowest singlet excited states (S_1) of corroles display higher fluorescence quantum yields (0.13-0.22) than that of the porphyrin,[11] and the T_1 state of corrole may react with oxygen ($^3\Delta_g$) producing singlet oxygen ($^1\Delta_g$) with a yield of 0.51-0.77. Halogen elements around corrole were proved helpful to increase the intersystem crossing (ISC) rate constant via heavy-atom effect.[12, 13] . The selective iodinated aluminum and gallium corroles display prompt fluorescence, phosphorescence, and delayed thermal fluorescence at room temperature.[14] In addition, it was observed variation of the substitution on the phenyl group in corroles will cause bigger changes in optical bands than those corresponding porphyrins. On the other hand, corrole exhibits striking solvent-dependent behavior.[15]

Although many investigations of the structure-function relationships of corroles have provided a wealth of information about the photophysical and photochemical properties of the S_1 and T_1 state, only a few of works focused on the higher excited electronic states as follows. The fluorescence from S_2 (the second excited singlet state) of Al(tpfc)(py) and Ga(tpfc)(py) was successfully observed using femtosecond fluorescence up-conversion methods.[16] The femtosecond polarization resolved VIS-pump IR-probe spectroscopy was combined with DFT calculations to identify and assign absorption bands of electronic transitions for aluminum corroles. [17]

On the other hand, research on fluorinated porphyrins, phthalocyanines, chlorines and corroles may be traced back 20 years ago due to their potential applications in photodynamic therapy, diagnosis and as models of naturally occurring compounds.[18] It was found that the electron-donating methoxy group -OCH3 in tetra (3-methoxyphenyl)porphyrin (TPPM) increases the singlet oxygen generation. However, additional introduction of fluorine atoms into phenyl ring of TPPMF has little influence on singlet oxygen generation.[19] Cavaleiro *et al*. studied meso-tetraphenylporphyrin and meso-pentafluorophenyl porphyrin and their copper complexes.[20] On the contrary, they found that the fluorinated derivatives exhibit a larger intersystem crossing and singlet oxygen production as compared to nonfluorinated derivatives. Another investigation also showed that the number and the position of the fluorinated substituents have significant influence on the singlet oxygen quantum yield. [21] Thus, the effect of fluorination on the singlet oxygen production by porphyrinoids is still not fully understood.

Recently, we performed the luminescence, excited triplet state absorption, and singlet oxygen generation measurements of fluorinated free base corroles and its gallium complexes.[22] The molecular structures of these free base fluorinated corroles are shown in scheme 1. We found $F_{10}C$ exhibits the highest quantum yield of singlet oxygen and ISC rate constant (k_{ISC}), which indicates that the peripherally flurophenyl substitution improve the ISC process. However, we cannot understand why the k_{ISC} of $F_{15}C$ is smaller than that of $F_{10}C$. The k_{ISC} does not totally follow the trend of the increase of the atomic number of the peripherally fluorine atoms, which indicates some other mechanisms are involved in. Moreover, how does the peripherally flurophenyl substitution influence the relaxation progress from higher excited electronic states to S_1 state is still unknown.

In this article, we wish to report the femtosecond time-resolved difference absorption spectroscopy of these corroles. The ultrafast relaxations: $S_2 \rightarrow S_1^*$, $S_1^* \rightarrow S_1$ and $S_1 \rightarrow T_1$ from femtosecond to nanosecond time domain are all recorded directly. Possible mechanisms to explain the relationship between the flurophenyl substitution and photophysical properties are discussed.

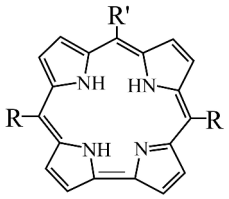

F_0C **R=R'=C_6H_5**
F_5C **R=C_6H_5** **R'=C_6F_5**
$F_{10}C$ **R=C_6F_5** **R'=C_6H_5**
$F_{15}C$ **R= R'=C_6F_5**

Scheme 1. The structure of F_0C, F_5C, $F_{10}C$ and $F_{15}C$.

Experiment:

The investigated corroles were synthesized according to the procedures described in the literature.[23] The steady-state absorption and emission spectra were measured using a PerkinElmer Lambda 850 UV-Vis Spectrometer and a PerkinElmer LS55 Luminescence Spectrometer (PE Company, USA), respectively.

The femtosecond transient absorption measurements were described earlier.[24] Briefly, the femtosecond time-resolved absorbance difference spectrometer employed a regenerative Ti:sapphire amplifier laser with 500 Hz repetition (Legend Elite USP HE+ , Coherent, 35 fs, 800 nm) as the primary laser source. The output beam was split into two. One with a power of 6 μJ/pulse was focused onto a pure water to generate a white light continuum as a probe beam. The other beam was frequency doubled by a 150 μm BBO crystal to gernerate 400 nm pump beam, and then passing a translation stage. An optical parametric amplifier (OPerA Solo) was used to generate 415 nm pump beam when the concentration of the sample was lowered to 10 μM. A mechanical chopper was employed to modulate the pump repetition frequency to 1/2 the probe repetition rate. The pump and probe pulses were focused to a diameter of 500 and 200 μm, respectively, at the flow cell interface by two plano-concave mirrors. The probe pulse was recorded by a fiber spectrometer (Avantes, AvaSpec_ULS2048L-USB2) at external trigger mode. The polarization of the pump beam was set to the magic angle (54.7°) with respect to the probe beam. The optical path in samples was 2 mm. Pump energy was 2 μJ/pulse. UV-visible absorption spectra of the samples before and after the experiments showed almost no change. The reported uncertainties in fit parameters were estimated 90% confidence limits based on reproducibility from fitting a number of independently measured transients.

The lifetime of S_1 fluorescence was detected by photomultiplier tube (Hamamatsu, R3809U-50) and measured by TCSPC (Becker & Hickl GmbH simple Tau152). Mai Tai SP was used as laser source.

Figure 1. UV-vis absorption spectra of the four corroles in toluene. Concentration is 25 μM.

Results:

1. Steady state spectra

Gouterman's four-orbital model is generally used to depict UV-Vis characteristics of porphyrinoid. Though corrole is in lack of a meso methine unit and possess a low symmetry (C_s), the four orbital model was also confirmed to hold well for corrole. [25,26] Therefore, the absorption bands around 420 nm are assigned to Soret bands and the moderately intense absorptions in the range 500-700 nm are assigned to Q bands as shown in Figure 1. The Q absorption bands and fluorescence spectra of investigated corroles are shown in Figure 2.[27] There is no obvious difference in Soret bands, except a slightly splitting for F_5C and $F_{15}C$, while no apparent splitting for F_0C and $F_{10}C$. Gaussian function was used to fit the multiple overlapping peaks and the fitting curves are represented by green solid lines in

Journal Name RSCPublishing

ARTICLE

Table 1. Absorption and fluorescence peaks of free base corroles in toluene at 295 K.

	Absorption Peaks (nm)				emission, λ_{max} (nm)	
	Soret band	Q bands				
		T2 (0 →1)	T2 (0→ 1)	T1(0 → 0)	T1(0 →0)	T2(0 →0)
F_0C	420	573	618	650	663	-
F_5C	419	578	611	642	654	-
$F_{10}C$	416	563	616	642	655	-
$F_{15}C$	413	567	608	634	644	615

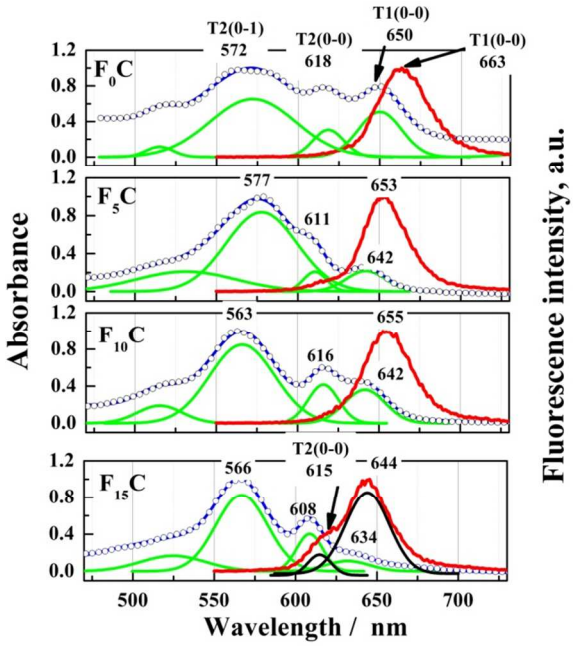

Figure 2. Normalized emission and absorption spectra of Q band in toluene (open circle). Emission spectra were measured with excitation at 560 nm (red solid). The emission spectra of F_0C, F_5C and $F_{10}C$ are approximately single bands. $F_{15}C$ exhibits a primary band and a shoulder located at 615 nm. Gaussian functions are used to fit the multiple overlapping peaks of Q band (green solid) and emission spectra of $F_{15}C$ (black solid).

Figure 2 also. The assignment of Q band vibronic satellites of free base meso-pyrimidinylcorrole has been achieved recently.[25, 28] The absorptions of the corroles in this study (especially $F_{10}C$) are similar to those of meso-pyrimidinylcorroles. Similar Q band assignments may also be drew accordingly. $F_{10}C$ was chosen as example. The vibronic peak at 566 nm and a shoulder at 616 nm of $F_{10}C$ are assigned to (0, 0) and (1, 0) of T2 tautomer respectively. The weak band at 642 nm is attributed to (0, 0) of T1 tautomer. Fluorescence emission spectra of corroles in toluene solution at room temperature with excitation at 560 nm are also shown in Figure 2. In the fluorescence spectra, the primary band of the four corroles locate at around 650 nm, which is assigned to the (0, 0) of the T1 tautomer. Only $F_{15}C$ shows a weak band centered at 615 nm, which is attributed to (0, 0) of the T2 tautomer. The three other corroles do not exhibit this T2 band. Detailed assignments are summarized in Table 1. The absorptions of Q bands are blueshifted with the increase of flurophenyl substituents. There is also a blueshift of the fluorescence maximum peaks, from 663 nm of F_0C to 644 nm of $F_{15}C$, about 448 cm^{-1}.

2. Transient Absorption Studies

2.1 Ultrafast Transient Absorption characteristics

Ultrafast transient absorption (TA) spectroscopy of free base corroles upon Soret band excitation (λ=400nm) was conducted to study the internal conversion (IC) of $S_2 \rightarrow S_1$ and the vibrational relaxation in S_1. For clarity, $F_{10}C$ was chosen as example. Figure 3 shows a series of chirp-corrected time-resolved differential TA spectra of $F_{10}C$ in toluene. From 0 ps to 0.14 ps, a wide positive excited state absorption (ESA) band appears with a sharp minus peak at 457 nm and a tiny ground state bleaching (GB) at 432 nm. The 457 nm minus peak can be assigned as the impulsive stimulated Raman gain signal from the CH stretching modes of the solvent.[29] Then it comes up with a gradual rising of an intense ESA band centered at ca. 470 nm and a slight shoulder at ca. 533 nm. At the same time, three negative bands which are coincident with the Q band at 566 nm, 616 nm and 642 nm also arise. Thus, we can attribute the negative bands in Figure 3(c) to the ground state bleaching (GB) signal of Q-band absorption. In Figure 3(d), a negative band at 655 nm gradually appears after around 2 ps, which is coincident with the steady fluorescence peak, until later at 30 – 40 ps, it arrives at the negative maximum. Meanwhile, the Q bands GB

at 616 nm decrease drastically. This negative absorption band at 655 nm is attributed to stimulated emission (SE) from the S_1 state.

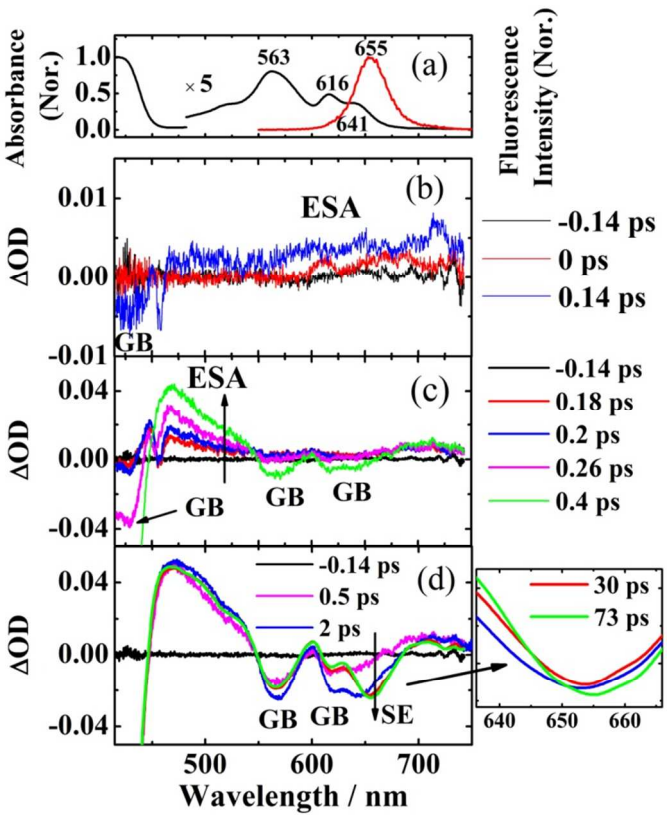

Figure 3. Femtosecond transient absorbance of 30 μM of $F_{10}C$ in toluene. Pump wavelength was 400 nm. (a) Normalized ground-state absorption (black solid line) and steady fluorescence (red solid line) in toluene. (b) Transient spectrum from 0 ps to 0.3 ps. (c) (c) Transient spectrum from 0.4 ps to 0.9 ps. (d) The comparison of transient spectrum between 2 ps and 73 ps.

Obviously, there are several transient states populated after the photoexcitation. The first transient species presents in Figure 3(b) should be S_2 state, because $F_{10}C$ is excited to its Soret band by 400 nm beam. The gradual rise of the SE and the decrease of 616 nm GB indicate that there is a vibrational relaxation in the S_1 state. Therefore, the TA showed in Figure 3(c) and Figure 3(d) from ca. 0.18 ps to 2 ps are attributed to the highly excited vibrational states of S_1 (S_1*). At last, the TA at 73 ps in Figure 3(d) should come from the lowest vibrational state in S_1.

Figure 4 presents the temporal profiles recorded at several selected wavelengths after photoexcitation of $F_{10}C$ in toluene along with the best-fit functions. At 687 nm, the temporal profile is associated with an initial rise of S_2 state with the instrument response time limit (~220 fs) followed by further biexponential decay with the lifetimes of about 0.6 ps and -22 ps (negative factor may be caused by the influence of SE signal, therefore, this lifetime is fixed during the curve fitting). From Figure 3, one can find that the ESA of S_2 state, SE and some transient species with longer lifetime (S_1* and S_1) overlap at 600 - 700 nm, which leads to the fact that the lifetime of 687 nm may not present real lifetime of S_2 state. Luckily, the main contributions to 470nm positive band are S_1* and S_1 and the tiny S_2 contribution can be neglected. The rising of 470 nm is therefore attributed to the decay from $S_2 \rightarrow S_1$*, about 0.19 ps lifetime with the instrument response time limit (~112 fs at 470 nm). There is another possibility that the observation of the decay of S_2 state is truly longer than the rise time of the S_1 state. (As we have fitted, 0.6 ps for the lifetime of S_2 and 0.19 ps for the rise time of S_1 state.) It suggests the S_2 of $F_{10}C$ may also contribute to its fluorescence, similar to Al(tpfc)(py) and Ga(tpfc)(py)[16] and meso-aryl-subporphyrins[30]. However, we failed to observe any S_2 fluorescence of $F_{10}C$ in toluene. The decay of $S_2 \rightarrow S_0$ is thus neglected of $F_{10}C$ in toluene.

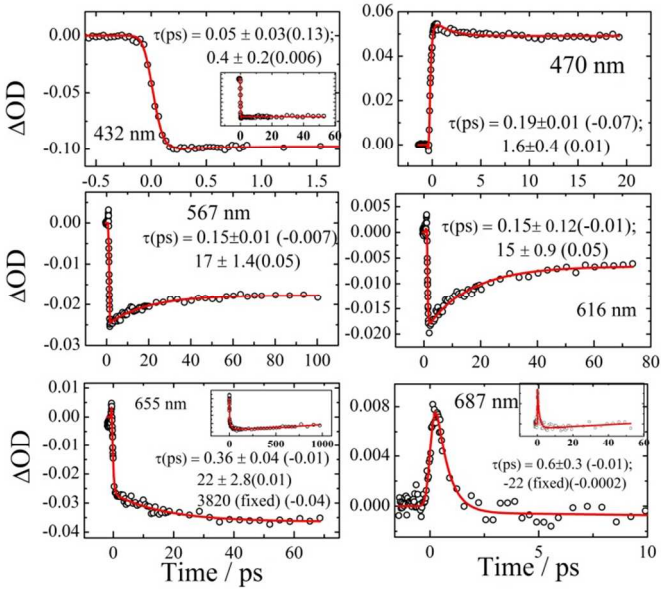

Figure 4. Time profiles at several selected wavelengths of 30 μM of $F_{10}C$ in toluene after 400 nm pump. Multiexponential fittings results of time constants (τ, ps) and amplitudes (in parentheses) are also shown in each sub figures.

The temporal profile of negative peak (SE) at ca. 655 nm can be fitted by a fast rise of 0.2 ps, a slow rise of 22 ps and a long decay, which are assigned to $S_2 \rightarrow S_1$*, S_1* $\rightarrow S_1$ and $S_1 \rightarrow S_0$, respectively. The longest lifetime is 3.82 ns, which is determined by measurement of S_1 fluorescence lifetime using TSCPC. The figures are shown in the Supporting Information (Figure S1). The temporal profiles of 567 nm and 616 nm include the initial rise of S_1* (ca. 0.15 ps) and the gradual decay of the Q band GB (ca. 15-17 ps). The 15-17 ps decay is simultaneous with the rise of 655 nm, which indicates that it is a population relaxation from S_1* $\rightarrow S_1$.

To investigate the effect of meso- flurophenyl substitution on the photophysical properties of corroles, TA spectra of F_0C, F_5C and $F_{15}C$ were also recorded. The corresponding spectra are shown in Supporting Information (Figure S2-S4). The TA assignments of F_0C, F_5C and $F_{15}C$ are similar with that of $F_{10}C$. Therefore, one can compare IC, vibrational relaxation and ISC of the four corroles.

2.2 The effect of flurophenyl substitution on the femtosecond and picosecond time domain

The comparison of the rise of S_1* (472 nm for F_0C, 470 nm for F_5C, 470 for $F_{10}C$, 456 nm for $F_{15}C$) is shown in Figure 5. The lifetimes of $S_2 \rightarrow S_1$* (τ_{IC}) may be obtained from the single exponential rise fitting with the convolution of the instrument response function and summarized in Table 2. The results indicate that the $S_2 \rightarrow S_1$* relaxation is shortened with the increasing of the flurophenyl substituent.

Another important relaxation S_1* $\rightarrow S_1$ is represented by the rise of SE as shown in Figure 6. This lifetime is dependent on the spectral

position of probe pulse. For example, the slow time constant for $F_{10}C$ is 17 ps at 567 nm, while it turns to 15 ps at 616 nm and 22 ps at 655 nm (Figure 4). To compare the lifetime of investigated corroles, we have chosen the lifetime of the peak of SE as an estimation of the time constant of $S_1^* \rightarrow S_1$, (SE peaks: 663 nm for F_0C, 654 nm for F_5C, 655 nm for $F_{10}C$ and 644 nm for $F_{15}C$, respectively). To get the maximum ΔOD, the samples are excited at 415 nm, where is near the absorption peaks of corroles. The time profiles were well fitted using a three-exponential decay. The longest lifetime was determined by the measurement of the fluorescence lifetime of S_1. The slower components are ca. 16 ps, 21 ps and 24 ps for F_5C, $F_{10}C$ and $F_{15}C$, respectively, which is assigned to the lifetime of $S_1^* \rightarrow S_1$ (τ_{VC}) (Table 2). F_0C exhibits some special features. Three lifetimes are 9 ps, 109 ps and 5.06 ns for F_0C and we assigned 9 ps to the lifetime of $S_1^* \rightarrow S_1$ temporarily. It will be introduced in detail in Section 2.4. Interestingly, the $S_1^* \rightarrow S_1$ time constant is prolonged with the increasing number of flurophenyl substituents.

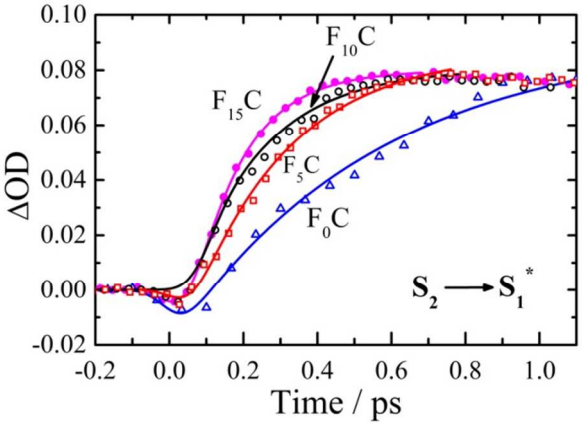

Figure 5. Comparison of IC from S_2 to S_1^* of F_0C, F_5C, $F_{10}C$ and $F_{15}C$ in toluene. The concentrations were 30 μM. The samples were excited at 400 nm. Probe wavelength was at 472 nm for F_0C, 470 nm for F_5C, 470 for $F_{10}C$, 456 nm for $F_{15}C$.

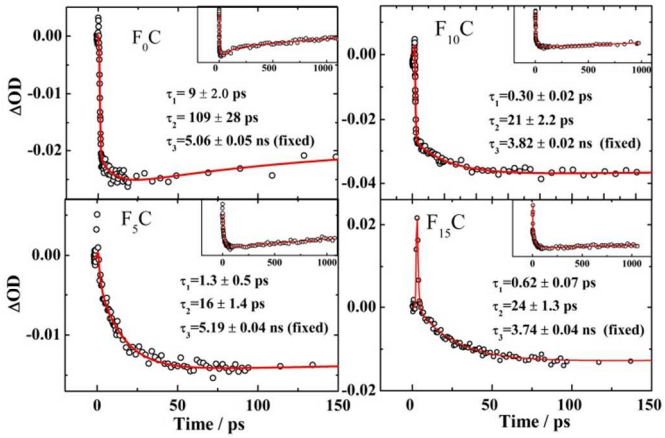

Figure 6. Comparison of SE rises of ca. 30 μM of F_0C, F_5C, $F_{10}C$ and $F_{15}C$ in toluene excited at 415 nm. The insets show the same signals on the nanosecond time scale. Red lines correspond to the three exponential fitting results.

2.3 The effects of flurophenyl substitutions on the nanosecond time domain

In order to unravel the influence of flurophenyl substitutions of on ISC process, TA transient absorption spectra of F_5C, $F_{10}C$ and $F_{15}C$ in toluene were obtained until 3.6 ns. The TA spectra and the time profiles of several key wavelengths were exhibited in Figure 7. The property of F_0C is different from the rest of flurophenyl substituted corroles. We will introduce it in the section 2.4.

One can notice that the time profiles at different wavelengths shows quite different features. It is because different lifetime components exhibit various weights at different wavelengths. The Soret bands of the corroles are located 420 nm. Therefore, the time profile of negative band at 434 nm is attributed to the ground-state absorption (abbreviated as "the S_0 bleaching") and is assumed to exhibit mainly the population changing of S_0 state. The SE decay at ca. 654 nm is assumed mainly to present the kinetics of S_1 state.

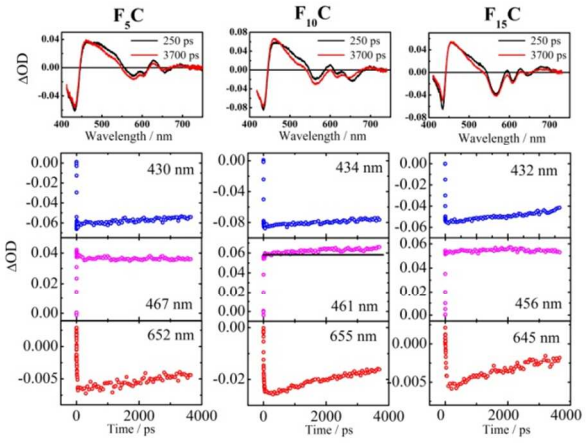

Figure 7. Comparison of 250 ps and 3700 ps transient absorbance of 30 μM of F_5C, $F_{10}C$ and $F_{15}C$ in toluene (upper pannal) and the time profiles of several key wavelengths (lower pannal). The samples were excited at 400 nm.

As seen in Figure 7, the lifetime of SE is shorter than that of the S_0 bleaching at ca 432 nm, which indicates that some excited molecules leave S_1 state, but they have not returned to S_0 state at the last detected time window, 3.7 ns. What is another energy dissipation channel besides IC and fluorescence? From our early study[22] and other papers[11, 31] corroles can arrive in its excited triplet state (T_1) after excited to the S_1 state and the TA spectra of $T_n \leftarrow T_1$ are also located at ca. 460 nm, [22] which overlaps with that of $S_n \leftarrow S_1$ absorption in this study. Therefore, the time profile of ca. 460 nm shown in Figure 7 exhibits a mixture of the decay of S_1 state and the rise of T_1 state.

The upper pannal of Figure 7 shows a comparison of TA spectra between 250 ps and 3.6 ns. The process of vibrational relaxation should have finished at 250 ps, thus, it presents mainly $S_n \leftarrow S_1$ absorption at this time window. The final TA spectra detected at 3.6 ns already contains some contribution from T_1 state.

We performed a global fitting procedure based on the singular value decomposition analysis (SVD) to distinguish the transient species[32]. Briefly, the TA spectra has a dimension of 1170 data points in the 417-750 nm spectral region, and 107 data points in the -0.5 ps to 3.6 ns. We proposed the kinetic scheme in Scheme 2 for the photophysics of F_5C, $F_{10}C$ and $F_{15}C$. In this proposed kinetic scheme, S_2 is neglected. One reason is that the absorption of S_2 is so small and decay rapidly, and SVD treats them as noises. Another is that the global fitting until nanosecond is so long that the

Journal Name RSCPublishing

ARTICLE

Table 2. Time Constants of corroles from Least-Squares Fits of Measurements

	ΔE $(S_2\text{-}S_1^*)$ cm^{-1}	τ_{IC} [a] (fs)	τ_{VC} (ps) [b]	k_1+k_2 $(10^8\ s^{-1})$ [c]	$k_1+k_T \approx k_1$ $(10^8\ s^{-1})$ [d]	k_T $(10^6 s^{-1})$ [e]	$k_2 = k_{ISC}$ $(10^8\ s^{-1})$ [f]	Calculated k_{ISC} $(10^8\ s^{-1})$ [g]
F_0C	6358	550± 57	9 ± 2.0	—	—	6.71	—	0.71
F_5C	6565	270± 20	16 ± 1.4	1.1 ± 0.35	0.32 ± 0.02	5.21	0.8 ± 0.4	1.21
$F_{10}C$	6276	190 ± 7	21 ± 2.2	2.3 ± 0.37	0.29 ± 0.01	4.59	2.0 ± 0.4	1.62
$F_{15}C$	6576	140 ± 6	24 ± 1.3	1.8 ± 0.5	0.64 ± 0.02	4.15	1.2 ± 0.5	1.24

[a] Time constants of internal conversion from $S_2 \rightarrow S_1^*$. [b] Time constants of vibrational cooling process ($S_1^* \rightarrow S_1$) [c] Time constant of the decay of S_1 which obtained by SVD and global fitting in the present study. [d] Time constants of the relaxation from by fitting 432 nm the S_0 bleaching. [e] Time constants of the relaxation from $T_1 \rightarrow S_0$ observed in ref [22]. [f] Time constants of intersystem crossing from $S_1 \rightarrow T_1$ obtained by subtracting k_1 from k_1+k_2. The k_{ISC} for F_0C is so small that we cannot fit it accurately. [g] Calculated k_{ISC} as in ref [22].

femtosecond process cannot be fitted accurately. The population change of the individual species has been solved and is described by the following set of equations 1-3.

From global fitting, the k_1+k_2 can be determined. In addition, one can get the sum of the time constants of all of the pathways returning to S_0 by fitting 432 nm the S_0 bleaching directly. In the present study, it should be k_1+k_T. From the lifetimes of T_1 observed in aerated toluene, [22] k_T is calculated and summarized in Table 2. It should be noticed that $k_T << k_1+k_T$, thus, we assumed the time constants obtained by fitting the S_0 bleaching is mainly contributed from k_1. Therefore, k_2 can be determined by subtracting k_1 from k_1+k_2. The results are summarized in Table 2. The fitting parameters are shown in Supporting Information, Figure S5.

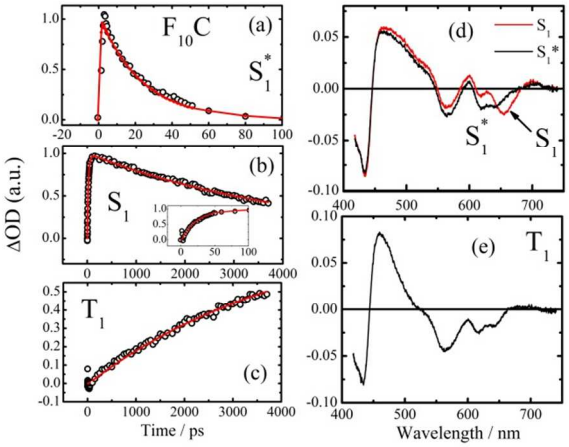

Figure 8. The results of the SVD and global-fitting analyses of TA spectra 30 μM of $F_{10}C$ in toluene, excited at 400 nm.

Figure 8 shows the Species-Associated Difference Spectra (SADS) of $F_{10}C$ in toluene (SADS of F_5C and $F_{15}C$ are shown in the Supporting Information (Figure S6-S7)). From Figure 8 (e), the difference between S_1^* and S_1 is moderate, except that S_1 exhibits the SE negetive band, while S_1^* does not. The 470 nm positive band of SAD of T_1 is narrower than that of S_1^* and S_1. These charterers are coordinate with TA spectra shown in Figure 3 and Figure 7, which proves that the SVD and global fitting get reasonable results. The ISC time constant is k_2, shown in Table 2. It shows that the k_{ISC} sequence from larger to smaller is $F_5C > F_{10}C < F_{15}C$.

Scheme 2: Relaxation Kinetics for the Excited Singlet Manifolds of F_5C, $F_{10}C$ and $F_{15}C$

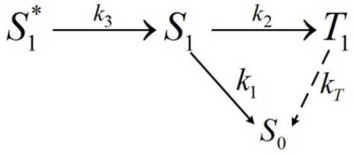

$$[S_1^*] = \exp(-k_3 t) \quad (1)$$

$$[S_1] = \frac{k_3}{k_1 + k_2 - k_3}[\exp(-k_3 t) - \exp(-(k_1 + k_2)t)] \quad (2)$$

$$[T_1] = \frac{k_2}{k_1 + k_2 - k_3}[1 - \exp(-k_3 t)] - \frac{k_2 k_3}{(k_1 + k_2)(k_1 + k_2 - k_3)}[1 - \exp(-(k_1 + k_2)t)] \quad (3)$$

$$[S_0] = 1 - \exp[-(k_1 + k_T)t] \approx 1 - \exp(-k_1 t) \qquad k_T \ll k_1 + k_T \quad (4)$$

Journal Name RSCPublishing

ARTICLE

2.4 Time profiles of F_0C

From our early study, the ISC quantum rate of F_0C in toluene is quite small. [22] In this regard, the observation of the time profiles of F_0C in toluene give us a unique opportunity to understand the mechanism of singlet electronic relaxation processes of corroles. The time profiles of F_0C in toluene (30 μM) excited by 415 nm are shown in Figure 9. One can notice that the time profile of 470 nm, exhibits biexponential decay (32 ps and 294 ps), which is different from other three corroles. The fast decay is independent of the pump energy from 3.2 μJ/pulse to 0.5 μJ/pulse, which indicates that it is not caused by singlet-singlet (S-S) annihilation (Supporting Information, Figure S8). In addition, the UV-Vis steady absorption does not exhibit the decrease of ε with the concentration increasing to 30 μM (Supporting Information, Figure S9). Therefore, the possibility of aggregation is also excluded.

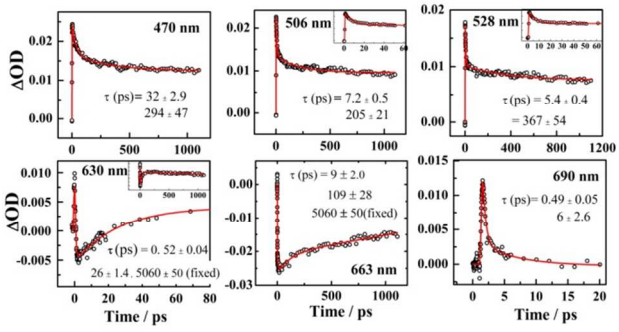

Figure 9. Time profiles at several selected wavelengths of 30 μM of F_0C in toluene after 415 nm pump. Multiexponential fittings results are also shown in each sub figures. When the time profile of 690 nm was performed, the concentration F_0C is diluted to 10 μM.

As seen in Figure 9, the observed fast lifetime of 470 nm depends strongly on the probe wavelength. From 32 ps at 470 nm, it turns to 7.2 ps at 506 nm and 5.4 ps at 528 nm, which is usually a feature of vibrational cooling.[33] Therefore, the fast component at 470 nm is denoted as the vibrational relaxation from $S_1^* \rightarrow S_1$. The second lifetime is several hundred picoseconds, which also appears at several other wavelengths. It is not the long decay of $S_1 \rightarrow S_0$, because the time profile of 663 nm cannot be well fitted by a biexponential decay, which also indicates the existence of this component. This hundred ps decay which follows the 9 ps of VC process were also attributed to an intermolecular VC process. It is because that vibrational cooling oftentimes is a muti-step energy transfer and exhibits a muti-exponential decay.

The negative band at 663 nm is attributed to stimulated emission (SE) from the S_1 state. The decay is far from complete at the final detected time window 1.2 ns. Therefore, the lifetime of S_1 state was determined to be 5.06 ns by fluorescence lifetime. 5.06 ns lifetime was fixed when the curve fitting was performed. Similar with $F_{10}C$, we observed a 0.49 ps fast decay on the red side of the TA spectra 690nm. It may also come from S_2 decay or intramolecular vibrational energy redistribution relaxation. This wavelength is measured at the concentration of 10 μM. Under higher concentration, the strong signal from S_1^* and S_1 will bury the weak decay.

For F_5C, $F_{10}C$ and $F_{15}C$, the time profiles of ca. 470 nm do not decay within the time scale of 3.7 ns. It may be caused by the overlap of the decay of S_1 and rise of T_1 at this wavelength. However, the time profile of 470 nm for F_0C exhibits biexponential decays, which indicates that there is little contribution from the rise of T_1 to 470nm. The ISC quantum yield is very small that we cannot use the model shown in Scheme 2 to calculate k_{ics} of F_0C. The main energy dissipation channel is $S_2 \rightarrow S_1^* \rightarrow S_1 \rightarrow S_0$, without ISC process for F_0C. Thus, the total sequence of ISC time constants from larger to smaller should be: $F_0C < F_5C < F_{10}C > F_{15}C$.

As regards the photostability of the corroles in toluene, only F_0C was found to be unstable: after ca. ten minutes of laser irradiation, the ΔOD is decreased by about 5 %. F_5C is more stable than F_0C, but not as stable as $F_{10}C$ and $F_{15}C$. The photostability of these corroles strongly increases when electron-withdrawing substituents are present around corrole periphery are in great agreement with previous researches.[11, 34, 35]

Discussion:

1. $S_2 \rightarrow S_1$* Internal Conversion

The initial population of the S_2 state is followed by ultrafast internal conversion (IC) which can be recorded by both the decay of the S_2 band and the rise of the S_1 ESA band. Here we monitored the rise of ca. 470 nm ESA band (S_1 rise) to compare the lifetime of S_2 states. From Table 2, the lifetime of S_2 state is accelerated by the flurophenyl substitutions from 550 fs of F_0C to 140 fs of $F_{15}C$. For the purpose to understand the mechanism of flurophenyl substitutions, we calculate the energy gap $\Delta E(S_2\text{-}S_1)$ by differences in the steady absorption of S_2 and S_1 (T2 (0 →1)), shown in Table 2. The calculation shows very similar values of $\Delta E(S_2\text{-}S_1)$, therefore, an energy gap law argument[36] cannot be used to explain the acceleration of the radiationless decay from $S_2 \rightarrow S_1^*$ by flurophenyl substitutions. Liu *et al.* measured the dynamic behavior of Soret-excited ZnTPP(F_{20}) and ZnTPP.[37] They found the effect of perfluorination of phenyl groups results in a 6-fold increase in the rate of radiationless decay of ZnTPP(F_{20}) compared with ZnTPP. The S_2 lifetime of ZnTPP(F20) in ethanol is 0.46 ps and 2.35 ps for ZnTPP. Their explanation is that perfluorination results in a withdrawal of electron density from the macrocycle framework and leads to ruffling of the macrocycle, and the increase of non-planar accelerates the rate of radiationless decay. [38, 39] Our results confirm Liu's observation, but in a 4-fold increase for a 15 F atoms increase compared $F_{15}C$ with F_0C. Therefore, the flurophenyl substitutions may also increase non-planar structures and accelerate the IC of $S_2 \rightarrow S_1^*$ for the free base corroles in this study.

Anusha *et al.* observed the dynamics of 1 mM triphenyl corrole (TPC, it is the same with F_0C in the present study) in chloroform and recorded 2.4 ps and 47 ps biexponential decays.[40] They attributed the 2.4 ps to the $S_2 \rightarrow S_1^*$ process. Baskin *et al.* have estimated

vibrationally excited Soret → Q_y, Q_x and Q_y → Q_x electronic relaxation occurs in less than 100 fs for H_2TPP by the femtosecond up conversion fluorescence method, following excitation at 398 nm in benzene.[41] Transient absorption spectra of and dynamics of PPIX and hemin have been performed by Marcelli *et.al*.[42] They recorded a red-shifted ESA bands at 475 nm and 430 nm in PPIX and their attribution is that the two processes Q_y → Q_x and vibrational energy relaxation (VR) in the Q_x band occur with a comparable time constants, 350 fs ± 50 fs. For the corroles in the present study, we cannot distinguish the three processes mentioned above. No ESA shift was resolved in these experiments; however, we cannot exclude the possibility of a hundreds fs or shorter Q_y → Q_x process. We temporarily assigned the hundreds fs components observed in these experiments to the ultrafast process of $S_2 \rightarrow S_1^*$ IC. To analysis it accurately, higher time resolution pulses and Q-band excitation should be performed in the further.

2. Vibrational Relaxation

For large molecules in solvents, there are two vibrational energy relaxation (VR) processes: intramolecular vibrational energy redistribution (IVR) between different modes of the excited solute that usually occurs within 10-100 fs, preparing a "hot" species with a defined local temperature, and following vibrational cooling (VC) that usually occurs on time scales from one to a few tens of ps.[43] For $F_{10}C$, the comparison of different TA spectra at several given time points are shown in the right panel of Figure 3. We found that there is in lack of isosbestic point. Besides, vibrational cooling usually presents different observed lifetimes at various spectral position of probe pulse.[33] This phenomenon was also observed from the time profiles of $F_{10}C$, especially F_0C. The wavelength-dependent lifetime and the lack of isosbestic point ascribed largely to vibrational cooling for large molecules.[33, 44-46] Thus, the gradual rise of the SE peak shown in Figure 6 can be interpreted as a VC process. From Table 2, VC process (τ_{VC}) is slowed down by the flurophenyl substitutions from 9 ps for F_0C to 24 ps for $F_{15}C$. The mechanism we proposed is as follows: The steady absorptions shown in Figure 2 have presented blue-shift of the Q bands induced by the flurophenyl substitutions, which may also increase the energy gap between the Franck-Condon active mode and the instantaneous normal modes of the solvent and result in longer VC time for the flurophenyl corroles.[47]

3. Intersystem Crossing

Recently, we obtained triplet state transient absorption spectra of corroles by the laser flash photolysis and calculated the triplet quantum yield Φ_T and of k_{ISC} by comparative actinometry method.[22] This method is influenced so much by the oxygen concentration in solution. In the present study, k_{ISC} fitted by SVD and global fitting in the present study are shown in Table 2, which give us another way to check the former results.

For comparison, the previously calculated k_{ISC} are also shown in Table 2. Though some difference exist, the obtained sequence of k_{ISC} (from larger to smaller) from both of the methods is $F_0C<F_5C<F_{10}C>F_{15}C$, which means that $F_{10}C$ presents the fastest ISC process. It suggests that the heavy atom effect induced by the fluorine atoms can enhance the intersystem crossing (ISC) probability via spin−orbital coupling. However, k_{ISC} of $F_{15}C$ is smaller than that of $F_{10}C$. The k_{ISC} does not totally follow the trend of the increase of the atomic number of the peripherally fluorine atoms, which indicates some other mechanisms are involved in. To understand that deeply, we compared the time profiles of GB at Soret band (432 nm for both of the sample) of $F_{10}C$ and $F_{15}C$ in Figure 10. It is assumed to exhibit mainly the population relaxation of S_0 state. The decay of 432 nm within nanosecond time scale should be mainly attributed to $S_1 \rightarrow S_0$, as mentioned above. We fitted the Soret band GB from 50 ps to 3.6 ns by single exponential function (k_1 in eq.1) and summarized the results in Table 2. From Table 2, k_1 of $F_{15}C$ is larger than that of $F_{10}C$ and F_5C, while that of $F_{10}C$ and F_5C are very similar. It indicates that more fluorine atoms induce an acceleration of the decay from $S_1 \rightarrow S_0$.

The possible explanation is that electron-withdrawing of perfluorination of phenyl groups increase the nonplanar distortion of macrocycle and accelerates the rate of decay from $S_1 \rightarrow S_0$, just as that of $S_2 \rightarrow S_1^*$. The ISC and decay (IC and FL) from $S_1 \rightarrow S_0$ compete with each other. Therefore, the heavy atom effect and the electron-withdrawing effect together lead to the highest ISC of $F_{10}C$. Holen *et al.* have investigated nickel porphyrins. They demonstrated that the decay rates of intersystem crossing to the triplet manifold and the non-radiative decay rates can be increased by the nonplanarity induced by the sterically crowded peripheral substituents.[46] For the metal-free porphyrins, the nonplanar can also enhance the rates of both internal conversion and intersystem crossing.[48, 49]

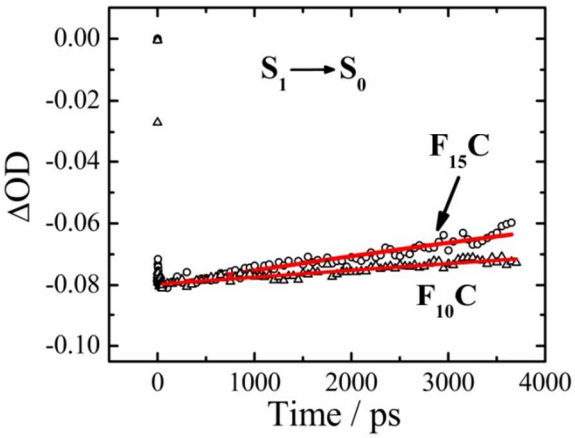

Figure 10. Time profiles of the $F_{10}C$ and $F_{15}C$ in toluene probed at 432 nm after pumping by 400 nm.

Conclusion:

In summary, we have investigated the ultrafast photophysical properties of a series of peripherally flurophenyl substituted free base corroles. With the use of femtosecond-resolved pump-probe transient absorption techniques, the dynamics of F_0C, F_5C, $F_{10}C$ and $F_{15}C$ in toluene were examined upon excitation at 400 and 415 nm in picosecond and nanosecond domain. Internal conversion from Soret (or S_2) to Q (or S_1), with time constants from 550 fs to 140 ps, is accelerated by the peripherally flurophenyl substitutions. On the contrary, the hot band S_1* exhibits vibrational cooling with time constant from ca. 9 ps to 24 ps. It is delayed by the peripherally flurophenyl substitutions. Additionally, in the nanosecond domain, we directly observed the ISC process of F_5C, $F_{10}C$ and $F_{15}C$, and confirmed $F_{10}C$ exhibits the highest time constant of ISC within these corroles. The possible explanation is that heavy atom effect increases the ISC from F_0C to $F_{10}C$, while electron-withdrawing of perfluorination of phenyl groups increase the nonplanar distortion of macrocycle and accelerates the rate of decay from $S_1 \rightarrow S_0$, which reduce the ISC again for the $F_{15}C$. It indicates that the electron-withdrawing of flurophenyl substitutions, together with heavy atom effect, influence the photophysical properties of excited states of corroles.

Acknowledgements

This work was supported by National Natural Science Foundation of China (Nos. 61475196, 61178037, 21171057 and 21371059), National Basic Research Program (973 Program) of China under Grant 2013CB922403, and the Open Fund of the State Key Laboratory of optoelectronic Materials and Technologies of Sun Yat-sen University (No. 2012-KF-MS2).

Notes and references

[a] State Key Laboratory of Optoelectronics Materials and Technologies, Sun-Yat Sen University, Guangzhou 510275, China

E-mail: stswh@mail.sysu.edu.cn

[b] Department of Chemistry, South China University of Technology, Guangzhou 510641, China.

E-mail: chhyliu@scut.edu.cn

References

1. H.-Y. Liu, M. H. R. Mahmood, S.-X. Qiu and C. K. Chang, *Coord. Chem. Rev.*, 2013, **257**, 1306-1333.

2. H. Agadjanian, J. J. Weaver, A. Mahammed, A. Rentsendorj, S. Bass, J. Kim, I. J. Dmochowski, R. Margalit, H. B. Gray, Z. Gross and L. K. Medina-Kauwe, *Pharm. Res.*, 2006, **23**, 367-377.

3. H. Agadjanian, J. Ma, A. Rentsendorj, V. Valluripalli, J. Y. Hwang, A. Mahammed, D. L. Farkas, H. B. Gray, Z. Gross and L. K. Medina-Kauwe, *Proc. Natl. Acad. Sci. USA*, 2009, **106**, 6105-6110.

4. Z. Gross, H. B. Gray, A. Zaban, J. R. Winkler, B. S. Brunschwig, A. Mahammed, S. Chappel and D. Walker, *Journal of Porphyrins and Phthalocyanines*, 2006, **10**, 1259-1262.

5. A. Mahammed, B. Mondal, A. Rana, A. Dey and Z. Gross, *Chem. Commun.*, 2014, **50**, 2725-2727.

6. F. D'Souza, R. Chitta, K. Ohkubo, M. Tasior, N. K. Subbaiyan, M. E. Zandler, M. K. Rogacki, D. T. Gryko and S. Fukuzumi, *J. Am. Chem. Soc.*, 2008, **130**, 14263-14272.

7. K. Peuntinger, T. Lazarides, D. Dafnomili, G. Charalambidis, G. Landrou, A. Kahnt, R. P. Sabatini, D. W. McCamant, D. T. Gryko, A. G. Coutsolelos and D. M. Guldi, *J. Phys. Chem. C*, 2013, **117**, 1647-1655.

8. L. Flamigni, D. Wyrostek, R. Voloshchuk and D. T. Gryko, *Phys. Chem. Chem. Phys.*, 2010, **12**, 474-483.

9. M. Tasior, D. T. Gryko, M. Cembor, J. S. Jaworski, B. Ventura and L. Flamigni, *New J. Chem.*, 2007, **31**, 247-259.

10. M. Tasior, D. T. Gryko, J. Shen, K. M. Kadish, T. Becherer, H. Langhals, B. Ventura and L. Flamigni, *J. Phys. Chem. C*, 2008, **112**, 19699-19709.

11. B. Ventura, A. Degli Esposti, B. Koszarna, D. T. Gryko and L. Flamigni, *New J. Chem.*, 2005, **29**, 1559-1566.

12. F. Nastasi, S. Campagna, T. H. Ngo, W. Dehaen, W. Maes and M. Kruk, *Photoch. Photobio. Sci.*, 2011, **10**, 143-150.

13. L. L. You, H. Shen, L. Shi, G. L. Zhang, H. Y. Liu, H. Wang and L. N. Ji, *Sci. China-Phys. Mech. Astron.*, 2010, **53**, 1491-1496.

14. J. Vestfrid, I. Goldberg and Z. Gross, *Inorg. Chem.* , 2014, **53**, 10536-10542.

15. T. Ding, E. A. Aleman, D. A. Modarelli and C. J. Ziegler, *J. Phys. Chem. A*, 2005, **109**, 7411-7417.

16. X. Liu, A. Mahammed, U. Tripathy, Z. Gross and R. P. Steer, *Chem. Phys. Lett.*, 2008, **459**, 113-118.

17. Y. Yang, D. Jones, T. von Haimberger, M. Linke, L. Wagnert, A. Berg, H. Levanon, A. Zacarias, A. Mahammed, Z. Gross and K. Heyne, *J. Phys. Chem. A*, 2012, **116**, 1023-1029.

18. T. Goslinski and J. Piskorz, *J Photoch. Photobio. C*, 2011, **12**, 304-321.

19. E. Zenkevich, E. Sagun, V. Knyukshto, A. Shulga, A. Mironov, O. Efremova, R. Bonnett, S. P. Songca and M. Kassem, *J. Photochem. Photobiol. B*, 1996, **33**, 171-180.

20. J. A. S. Cavaleiro, H. Görner, P. S. S. Lacerda, J. G. MacDonald, G. Mark, M. G. P. M. S. Neves, R. S. Nohr, H.-P. Schuchmann, C. von Sonntag and A. C. Tomé, *J. Photochem. Photobiol. A*, 2001, **144**, 131-140.

21. S. K. Pandey, A. L. Gryshuk, A. Graham, K. Ohkubo, S. Fukuzumi, M. P. Dobhal, G. Zheng, Z. Ou, R. Zhan, K. M. Kadish, A. Oseroff, S. Ramaprasad and R. K. Pandey, *Tetrahedron*, 2003, **59**, 10059-10073.

22. W. Shao, H. Wang, S. He, L. Shi, K. Peng, Y. Lin, L. Zhang, L. Ji and H. Liu, *J. Phys. Chem. B* 2012, **116**, 14228-14234.

23. P. Liang, H.-Y. Liu, L. Chen, F. Yam and C. K. Chang, *Chinese J. Inorg. Chem.*, 2009, **25**, 1420-1425.

24. L. Zhang, J. Yang, L. Wang, G.-Z. Yang and Y.-X. Weng, *J. Phys. Chem. B*, 2003, **107**, 13688-13697.

25. W. Beenken, M. Presselt, T. H. Ngo, W. Dehaen, W. Maes and M. Kruk, *J. Phys. Chem. A*, 2014, **118**, 862-871.

26. A. Ghosh, T. Wondimagegn and A. B. J. Parusel, *J. Am. Chem. Soc.*, 2000, **122**, 5100-5104.

27. C. K. Chang, P.-W. Kong, H.-Y. Liu, L.-L. Yeung, H.-K. Koon and N.-K. Mak, *Proc. of SPIE*, 2006, **6139**.

28. M. Kruk, T. H. Ngo, P. Verstappen, A. Starukhin, J. Hofkens, W. Dehaen and W. Maes, *J. Phys. Chem. A*, 2012, **116**, 10695-10703.

29. S. Yamaguchi and H.-o. Hamaguchi, *J. Chem. Phys.*, 1998, **109**, 1397-1408.

30. J. Sung, P. Kim, S. Saga, S. Hayashi, A. Osuka and D. Kim, *Angew. Chem. Int. Edit.*, 2013, **52**, 12632-12635.

31. S. Yamauchi, M. Tanabe, Y. Ohba, K. Sugisaki, K. Toyota, K. Sato, T. Takui and I. Saltsman, *Chem. Phys. Lett.*, 2012, **521**, 64-68.

32. J. P. Zhang, T. Inaba, Y. Watanabe and Y. Koyama, *Chem. Phys. Lett.*, 2000, **331**, 154-162.

33. C. T. Middleton, B. Cohen and B. Kohler, *J. Phys. Chem. A*, 2007, **111**, 10460-10467.

34. D. T. Gryko and B. Koszarna, *Synthesis-Stuttgart*, 2004, 2205-2209.

35. G. R. Geier, J. F. B. Chick, J. B. Callinan, C. G. Reid and W. P. Auguscinski, *Journal of Organic Chemistry*, 2004, **69**, 4159-4169.

36. S. Velate, X. Liu and R. P. Steer, *Chem. Phys. Lett.*, 2006, **427**, 295-299.

37. X. Liu, U. Tripathy, S. V. Bhosale, S. J. Langford and R. P. Steer, *J. Phys. Chem. A*, 2008, **112**, 8986-8998.

38. S. G. Dimagno, A. K. Wertsching and C. R. Ross, *J. Am. Chem. Soc.* , 1995, **117**, 8279-8280.

39. A. K. Wertsching, A. S. Koch and S. G. DiMagno, *J. Am. Chem. Soc.*, 2001, **123**, 3932-3939.

40. P. T. Anusha, D. Swain, S. Hamad, L. Giribabu, T. S. Prashant, S. P. Tewari and S. V. Rao, *J. Phys. Chem. C*, 2012, **116**, 17828-17837.

41. J. S. Baskin, H. Z. Yu and A. H. Zewail, *J. Phys. Chem. A*, 2002, **106**, 9837-9844.

42. A. Marcelli, P. Foggi, L. Moroni, C. Gellini and P. R. Salvi, *J. Phys. Chem. A*, 2008, **112**, 1864-1872.

43. J. Petersson, M. Eklund, J. Davidsson and L. Hammarstrom, *J Phys. Chem. B*, 2010, **114**, 14329-14338.

44. S. A. Kovalenko, R. Schanz, H. Hennig and N. P. Ernsting, *J Chem. Phys.*, 2001, **115**, 3256-3273.

45. R. Ghosh and D. K. Palit, *J Phys. Chem. A*, 2012, **116**, 1993-2005.

46. C. M. Drain, C. Kirmaier, C. J. Medforth, D. J. Nurco, K. M. Smith and D. Holten, *J. Phys. Chem.* , 1996, **100**, 11984-11993.

47. H. Z. Yu, J. S. Baskin and A. H. Zewail, *J. Phys. Chem. A*, 2002, **106**, 9845-9854.

48. S. Gentemann, C. J. Medforth, T. P. Forsyth, D. J. Nurco, K. M. Smith, J. Fajer and D. Holten, *J. Am. Chem. Soc.*, 1994, **116**, 7363-7368.

49. S. Gentemann, C. J. Medforth, T. Ema, N. Y. Nelson, K. M. Smith, J. Fajer and D. Holten, *Chem. Phys. Lett.*, 1995, **245**, 441-447.